A *Pn* magnitude scale $m_b(Pn)$ for earthquakes along the equatorial Mid-Atlantic Ridge

Won-Young Kim [ORCID],[1] Guilherme W. S. de Melo[2] and Marcelo Assumpção [ORCID][3]

[1]*Lamont-Doherty Earth Observatory, Columbia University,* 61 *Route* 9 *W, Palisades, NY* 10964*, USA. E-mail:* wykim@ldeo.columbia.edu
[2]*GEOMAR Helmholtz Centre of Ocean Research Kiel, Research Division* 4 *– Marine Geodynamics, Wischhofstrasse* 1-3, 24148 *Kiel, Germany*
[3]*Instituto de Astronomia, Geofísica e Ciências Atmosféricas, Universidade de São Paulo, São Paulo, SP, Brazil*

SUMMARY

We developed a short-period *Pn* magnitude scale $m_b(Pn)$ for earthquakes along the equatorial Mid-Atlantic Ridge. Due to low signal-to-noise ratios, teleseismic body wave magnitude and long-period surface wave magnitude cannot be confidently determined for small earthquakes of $m_b < 4$. Local magnitude scales are also not useful for these events because the oceanic environment does not allow the propagation of crustal phases. However, regional high-frequency *Pn* waves from these small- to moderate-size (m_b 3–6) earthquakes are well recorded in the equatorial Atlantic region and can be used to assign magnitudes. We measured over 2041 *Pn* peak amplitudes on vertical records from about 21 stations in northeastern Brazil and 11 stations in western Africa in the distance range of 700–3700 km. We analysed data from 189 events from the global centroid moment tensor catalogue to tie our $m_b(Pn)$ scale to M_w so that seismic moments can be readily estimated. *Pn* arrivals show apparent group velocity between 7.9 km s^{-1} at short ranges ($\sim$1000 km) and up to 9.1 km s^{-1} at 3500 km. The measured peak amplitudes have a frequency between 0.8 and 3 Hz at 1000–1800 km, but at greater distances, 1800–3700 km, they show a remarkably consistent frequency of about 0.8 Hz. The peak amplitude attenuates at a higher rate at short distances ($\sim$0.65 magnitude units between 700 and 2000 km) but attenuates at a lower rate at long distances ($\sim$0.35 magnitude units between 2000 and 3700 km). The low rate of amplitude decay with distance and nearly constant frequency content of the peak amplitudes suggest that *Pn* waves propagate efficiently in the lower part of the upper mantle in the equatorial Atlantic Ocean basins. These are important attributes of oceanic *Pn* waves that can be used to assign magnitude for small- to moderate-size earthquakes in the equatorial mid-Atlantic region. The estimated station corrections correlate well with upper mantle low-velocity anomalies, especially in Brazil.

Key words: Body waves; Earthquake ground motions; Seismic attenuation; Site effects.

1. INTRODUCTION

The equatorial Atlantic region consists of mid-ocean ridges and deep ocean basins, bounded by South America in the west and Africa in the east. Seismicity and tectonics in the region reflect the divergent plate boundary between the South American and African plates (Fig. 1). Spreading rates of the tectonic plates at the equatorial Mid-Atlantic Ridge (MAR) are low, and the plates move 23–31 mm yr^{-1} between Fifteen Twenty and Chain transform faults (e.g. DeMets *et al.* 2010). Slow-spreading equatorial MARs are offset by transform faults—some are the longest-offset transform faults on Earth. The detailed process of crustal accretion along the ridges and strike-slip faulting along the transform faults is still poorly understood, mainly due to the lack of close-in seismic and other geophysical observations. The region is seismically active,

with about 220 earthquakes per year with a magnitude greater than m_b 3.0, as reported in the International Seismological Centre (ISC) catalogue during 2010–2020. The seismicity provides an opportunity to unravel the poorly known tectonic processes of the equatorial MARs and transform faults.

A comprehensive description of seismicity may encompass the detection, location and magnitude (*size*) assignment of earthquakes. The seismicity in the equatorial Atlantic region is monitored by the land stations of the Brazilian Seismographic Network (RSBR; Bianchi *et al.* 2018). For example, earthquakes in the Doldrums transform system have an event detection magnitude threshold of m_b 3.7 (Fig. 1), and the detection threshold is m_b 3.5 for the 4–5°N ridge (de Melo *et al.* 2021a), and m_b 3.4 in the St Paul transform system (e.g. de Melo & do Nascimento 2018).
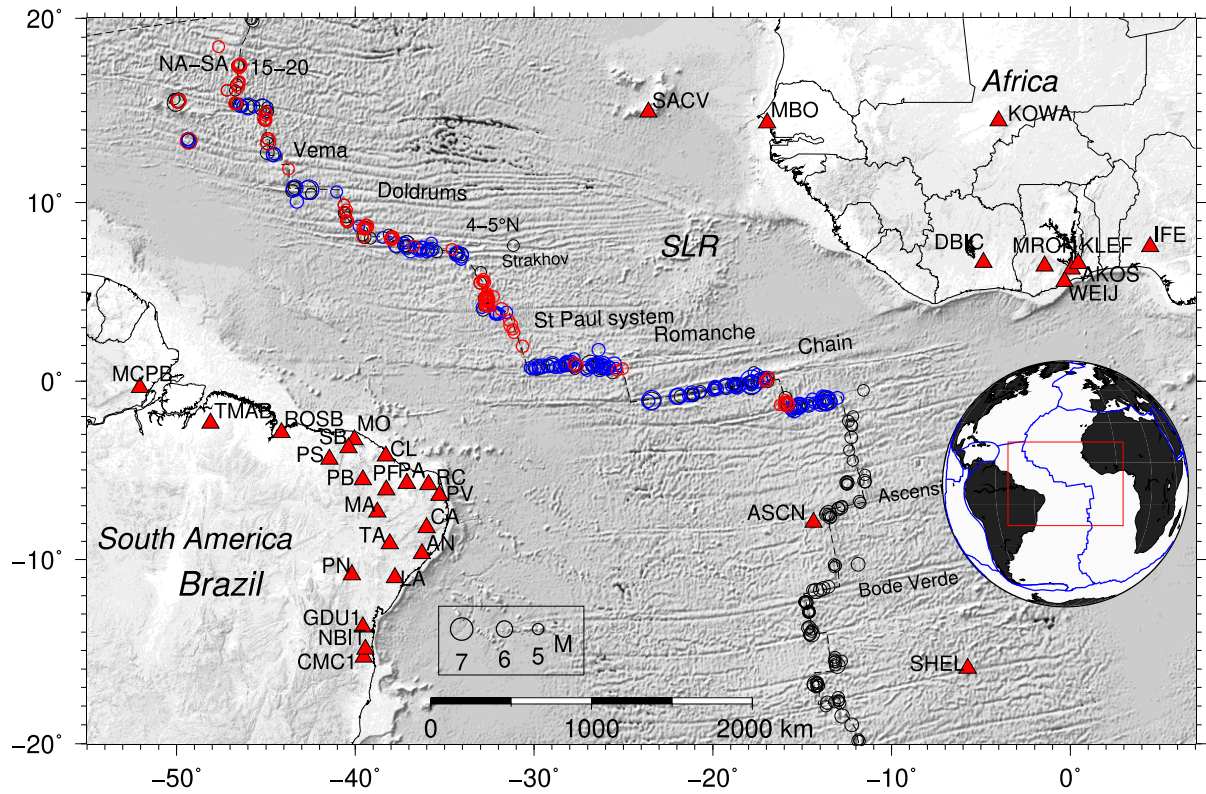
Figure 1. Epicentres of 1627 earthquakes with $m_b \geq 4.0$ that occurred along the equatorial MARs during 2010–2020, reported by the International Seismological Centre (ISC), are plotted by *circles*. Symbol size is proportional to event magnitude (m_b). 32 seismographic stations used are plotted by *red triangles*. 189 earthquakes from the global centroid moment tensor solution (GCMT) catalogue are selected for analysis. Among the events, 112 strike-slip events that occurred along the transform faults are plotted by *blue circles*, whereas 77 normal-faulting events along the spreading ridges are plotted by *red circles*. Earthquakes that occurred along transform faults between the Fifteen-twenty (15–20) in the north and Chain fracture zones in the equatorial region are selected for analysis because stations in northeastern Brazil could not analyse events that occur farther south.

The Brazilian network assigns magnitudes of those earthquakes that occur in equatorial MAR using the teleseismic scale (m_b) or the regional magnitude scale, mR (Assumpção 1983) without any specific calibration for the predominantly oceanic paths across the equatorial Atlantic. Hence, there is a need to find a suitable method to assign a reliable magnitude to those earthquakes in the equatorial MAR.

The purpose of magnitude scales is to facilitate quantitative analysis of the size of seismic events, which can be achieved in two fundamentally different ways. The first method has been an empirical approach, in which the strength of ground motion from an event is measured in a preset time window and frequency band, and the event magnitude is assigned through a process that accounts for the instrument response; ground motion decays with distance from the event and taking the average across the network of seismic stations. Several empirical magnitude scales have been developed using the various observed seismic waves.

A second method to assign event size using a physical approach had been initiated in the 1960s by Aki (1966). He introduced seismic moment, M_0 (in units of Newton-metre), as a parameter for assigning event size using the strength of an equivalent double couple acting at the source. Since M_0 is proportional to the fault area times the average slip, the seismic moment can uniformly relate information from plate tectonics and historical and modern seismology. The moment magnitude, M_w, is introduced by Kanamori (1977), which relates to M_0 [via local magnitude M_L] as $M_w = (2/3)$ $\log_{10} M_0$ [N-m]–6.033.

For earthquakes with $m_b > 4$, magnitudes derived from surface wave (M_S) and teleseismic body-wave (m_b) can be used to quantify ground motion. But for small events ($m_b < 4$), surface- and body-wave amplitudes are usually below noise level at far regional distances. Thus, seismic waves at distance ranges of a few hundred up to about 4000 km must be used for event quantification, namely, *Pn* and *Sn* waves. *Pn* is a refracted wave propagating mostly along the uppermost mantle and then returning to the crust at the critical incidence. *Pn* is less affected by the crustal structure along the paths, and for earthquakes in oceanic regions, high-frequency *Pn* and *Sn* waves (0.5–10 Hz) are the most prominent regional seismic waves. They can be used to assign the magnitude of small-to-large earthquakes (magnitude M_w 3.5–7), as shown by Kim & Ottemöller (2017).

In this paper, we developed an empirical magnitude scale based on observations of the *Pn* wave. We established a method to estimate moment magnitudes for earthquakes on spreading ridges and transform faults from *Pn* waves. Although M_w may be regarded as a more robust measurement of earthquake size since it is a more physically based measurement than other magnitude scales in use, $m_b(Pn)$ can be readily available for many events of $m_b < 5$. Moreover, $m_b(Pn)$ is assigned from short-period signals and is thus distinctly different from M_w values which are estimated from long-period signals. Therefore, two events of the same moment can have different $m_b(Pn)$. Assigning several types of magnitude to an earthquake allows for a greater understanding of the earthquake source. We contribute to understanding current tectonics and assist in

evaluating hazards from large earthquakes in the equatorial Atlantic region (Fig. 1).

The main objectives of this paper are (1) to develop a magnitude scale based on *Pn* waves that can be used for small offshore earthquakes (less than m_b 4.0) along equatorial MAR observed at land stations in northeastern Brazil and western Africa and (2) to estimate the seismic moment of those small earthquakes directly from the observed $m_b(Pn)$ body-wave magnitudes.

2. DATA

We selected 189 earthquakes that occurred along the equatorial MARs from 2011 to 2019 from the global centroid moment tensor solution (GCMT) catalogue. Events were selected for even geographic distribution along the equatorial MAR from 15–20 Ridge in the north to the Chain transform fault in the south, and events that produced an adequate number of records with a high signal-to-noise ratio (SNR). 112 earthquakes are strike-slip events on transform faults, and 77 events are normal faulting events along spreading ridges (see Fig. 1). Magnitudes range from M_w 4.95 to 7.14, and all events generated *Pn* waves with high SNR, as shown in Fig. 2. Amplitude measurements with high SNR are essential to determine a reliable amplitude–distance curve for the magnitude scale. The GCMT events are utilized to calibrate the new empirical magnitude scale to moment magnitude. We can also assess source effects on observed *Pn* amplitudes since we know all their source mechanisms.

The selected GCMT events also have location estimates from the ISC and the Preliminary Determination of Epicentres (PDE). As pointed out by Kim *et al.* (2020), PDE locations align in ways that are more tectonically consistent and correlate better with bathymetric features and focal mechanism types. Although location uncertainty is not important in developing a magnitude scale, absolute locations matter in later sections when we come to group earthquakes with specific source mechanisms into source regions in order to interpret the way in which different mechanisms influence the observed peak amplitude measurements. We took the PDE locations as our primary event locations, as given in Table S1.

We analysed *Pn* waves recorded by broad-band stations in northeastern Brazil (RSBR; Bianchi *et al.* 2018), Global Seismographic Network (GSN; Ringler *et al.* 2022) and AfricaArray in western Africa (see Data Availability). We analysed data from 21 stations in the west, eight stations in the east of equatorial MAR, and three stations on islands in the equatorial Atlantic region. Stations and their network affiliations are listed in Table 1 and plotted in Fig. 1. *Pn* paths used in this study are plotted in Fig. 3.

2.1 *Pn* waves from earthquakes along the equatorial MARs

In the equatorial Atlantic region, *Pn* waves propagate mostly in the oceanic mantle lid beneath ocean basins, such as the Sierra Leone Rise (SLR, Fig. 1), with a segment of the ray path in the transition zone from oceanic to continental crust (to the recording station on land).

Examples of records with *Pn* waves are shown in Fig. 2 to illustrate the waveform data being utilized to develop the regional *Pn* magnitude scale. Three-component broad-band traces from an M_w 6.5 earthquake in the Romanche transform fault on 30 November 2017 recorded at stations in Northeastern Brazil are plotted on apparent group velocity axis. Raw broad-band records show

that long-period surface waves are the predominant signals at these stations at far regional distances (1600–1700 km) from this shallow earthquake (Fig. 2a), whereas three-component records at the high-frequency band (0.5–15 Hz; simulated high-frequency Wood–Anderson records) show clear regional *Pn* (at ∼8 km s^{-1}) and *Sn* (at ∼4.5 km s^{-1}) waves (Fig. 2b). We utilize these high-frequency regional *Pn* waves to assign magnitudes for small- to moderate-size earthquakes.

3. METHODS

3.1 *Pn* peak amplitude measurement

We follow Kim & Ottemöller (2017) and simulated the vertical component Wood–Anderson (WA) seismogram by converting the original record to that of a standard WA torsion seismograph response (natural period, $T_0 = 0.8$ s; damping constant, $h = 0.7$; Anderson & Wood 1925) with a magnification of unity so that amplitude is in nanometres (Richter 1935; Uhrhammer & Collins 1990).

We measured the maximum zero-to-peak amplitude of the *Pn* phase and refer to it as the '*peak amplitude*' throughout this study. The peak amplitude is measured for a time window starting from the first arrival *Pn* phase down to an apparent group velocity of ∼6.0 km s^{-1} (Fig. 2). In the equatorial Atlantic region, the *Pn* peak amplitude corresponds from 7.0 to 8.0 km s^{-1} in the distance up to 2000 km. However, the apparent group velocity increases gradually and reaches 9.1 km s^{-1} at 3500 km. This reflects the ray paths extending to a deeper part of the mantle with higher *P*-wave velocity.

We measured 2041 *Pn* peak amplitudes on vertical records from 189 selected events in the 700–3700 km distance range. The logarithms of the peak amplitudes in nanometres are normalized by subtracting the moment magnitudes and are plotted against epicentral distance in Fig. 4. Our next step is to turn such measurements into station and network magnitudes.

3.2 *Pn* magnitude scale $m_b(Pn)$

We develop $m_b(Pn)$ for the equatorial Atlantic region by following a method nearly identical to that developed by Kim & Ottemöller (2017) for $m_b(Pn)$ scale in the northern Atlantic region. They introduced the following $m_b(Pn)$ magnitude scale,

$$m_b(Pn) = \log_{10} A - \log_{10} A_0(\Delta) + C, \tag{1}$$

where A is the peak *Pn* wave amplitude on a simulated vertical WA record in nm, Δ is the epicentral distance in kilometres, $\log_{10} A_0(\Delta)$ is the empirically derived amplitude–distance curve to correct for *Pn* wave amplitude loss along the propagation path in nm, and C is the station correction that accounts for local site and upper-mantle conditions at seismic stations. The core of the magnitude scale is the amplitude–distance curve,—$\log_{10} A_0(\Delta)$, that compensates for seismic wave amplitude decay with distance. The amplitude–distance curve can be represented by a power law dependence on distance accounting for *Pn* upper mantle path along the oceanic upper mantle lid (e.g. Chun *et al.* 1989) plus anelastic attenuation and the geometrical spreading of *Pn* in the crustal legs. Hence, $\log_{10} A_0(\Delta)$, can be expressed as:

$$\log_{10} A_0(\Delta) = b \log_{10}(\Delta_{ref}/\Delta) - 2.04, \tag{2}$$

where b is the slope for the *Pn* amplitude–distance curve in the oceanic upper mantle lid, Δ_{ref} is the reference distance of 100 km
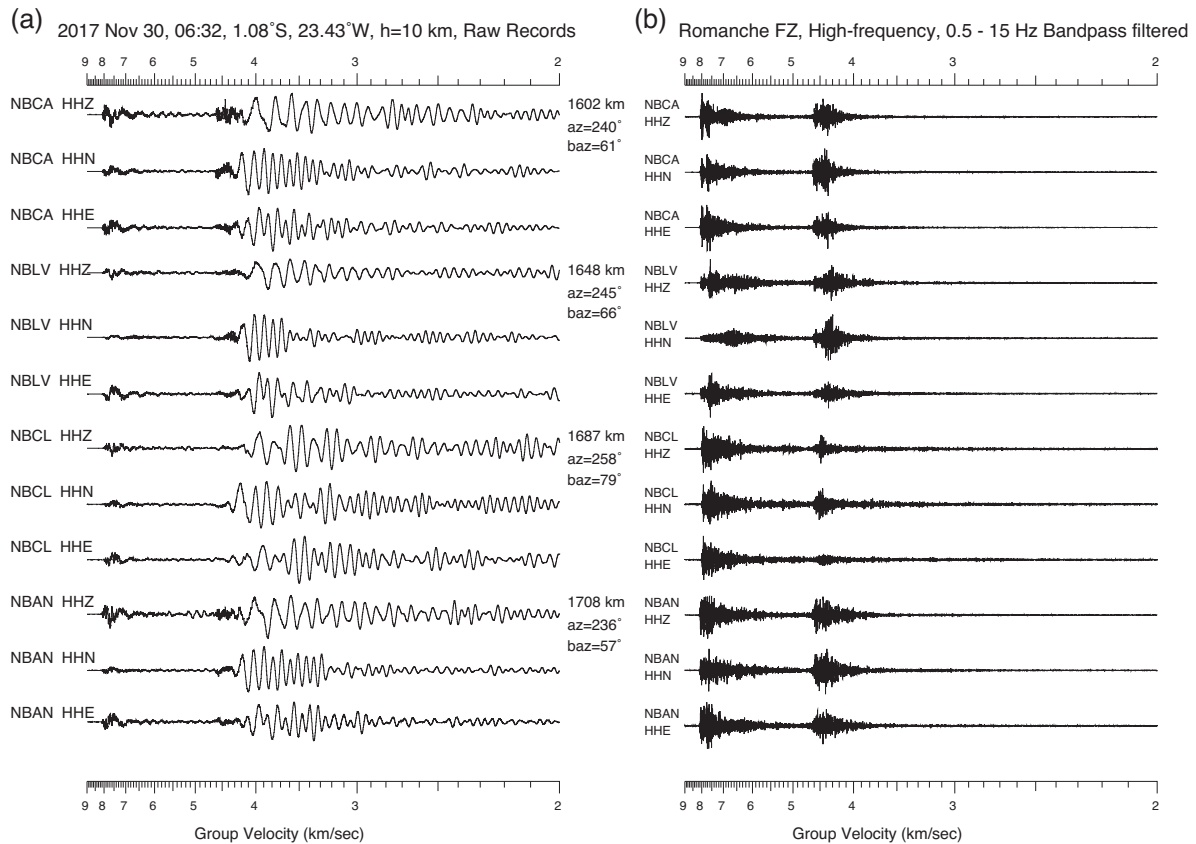
Figure 2. (a) Three-component broad-band seismograms recorded at stations in Northeastern Brazil from an M_w 6.5 earthquake that occurred in the Romanche Fracture Zone on 2017 November 30 are plotted on the apparent group velocity axis (distance/time). Long-period surface waves are predominant signals recorded at these stations at far regional distances (1600–1700 km). (b) Three-component seismic records at the high-frequency band (0.5–15 Hz) show clear regional *Pn* (at ~8 km s^{-1}) and *Sn* (at ~4.5 km s^{-1}) waves. We utilize these high-frequency regional *Pn* waves to assign magnitude for small- to moderate-size earthquakes that occur along the equatorial MARs.

and –2.04 is the constant to account for *Pn* amplitude loss in the two crustal legs—one for a continental crustal leg beneath the station and the other from the source to the reference distance. The reference distance of 100 km is based on the *Pn* wave travel time cross-over distance of about 100 km in the equatorial Atlantic region. The constant –2.04 is composed of geometrical spreading of –$\log_{10}$ (100) (km) = –2.0 and anelastic attenuation of –0.04 (e.g. Boatwright 1994). The *Pn* wave attenuation is evaluated for a logarithmic centre frequency, f = 2 Hz (0.5–8 Hz), with an average oceanic crustal Q_P value of Q_0 (1 Hz) = 900 (Sereno & Orcutt 1987) and traveltime t_{ref} = 100 km/7.9 km s^{-1} (*Pn* wave with centre group velocity of 7.9 km s^{-1}). More details on the derivation of the constant 2.04 are given by Kim & Ottemöller (2017). By inserting the above amplitude–distance curve into eq. (1) we rewrite the *Pn* magnitude as,

$$m_b(Pn)_{ij} = \log_{10}A_{ij} - b\log_{10}\left(100/\Delta_{ij}\right) - C_i - 2.04, \qquad (3)$$

where $m_b(Pn)_{ij}$ is the station magnitude and indices *i* and *j* denote the *i*th station and *j*th event.

3.3 Inversion for station correction, amplitude–distance curve and event magnitude adjustment

We introduce the event magnitude adjustment (*E*) that represents differences between the long-period moment magnitude (M_w) and

the short-period *Pn* magnitude $m_b(Pn)$ for each event as

$$M_{Wj} = m_b(Pn)_j + E_j, \qquad (4)$$

where $m_b(Pn)_j = \frac{1}{N}\sum_{i=1}^{N} m_b(Pn)_{ij}$ is the network magnitude of the *j*th event, obtained by averaging over the *N* observing stations of the network. This adjustment is useful because it can be estimated from observations. By using *E*, we rewrite eq. (3) in a form that can be solved by the least-squares method as

$$\left[\log_{10}A_{ij} - M_{Wj}\right] = -b\log_{10}\left(100/\Delta_{ij}\right) - C_i - E_j - K, \qquad (5)$$

where the constant $K = 2.04 + K_0$, and we introduce a constant K_0 that gives the offset between M_w and $m_b(Pn)$ values. Initially, *K* is set to 2.04 for amplitude attenuation in the two crustal legs of the *Pn* path (Kim & Ottemöller 2017). In eq. (5), the parameters to be determined are the slope of the amplitude–distance curve (*b*), station corrections (C_i), event magnitude adjustments (E_j) and the constant (*K*). Since the equations of condition for this problem are linearly dependent, we assume the average station corrections and event magnitude adjustments to be zero ($\sum_i C_i = \sum_j E_j = 0$). Eq. (5) can be written in matrix form as $\Delta\mathbf{d} = \mathbf{A}\,\Delta\mathbf{p}$, which is a system of at least *I* (stations) + *J* (events) + 2 (the slope *b* and the constant *K*) linearly independent equations. $\Delta\mathbf{d}$ is the data residual [observed amplitude ($\log_{10} A_{ij}$—M_{Wj})—calculated amplitude], **A** is a matrix of partial derivatives of calculated amplitude with respect

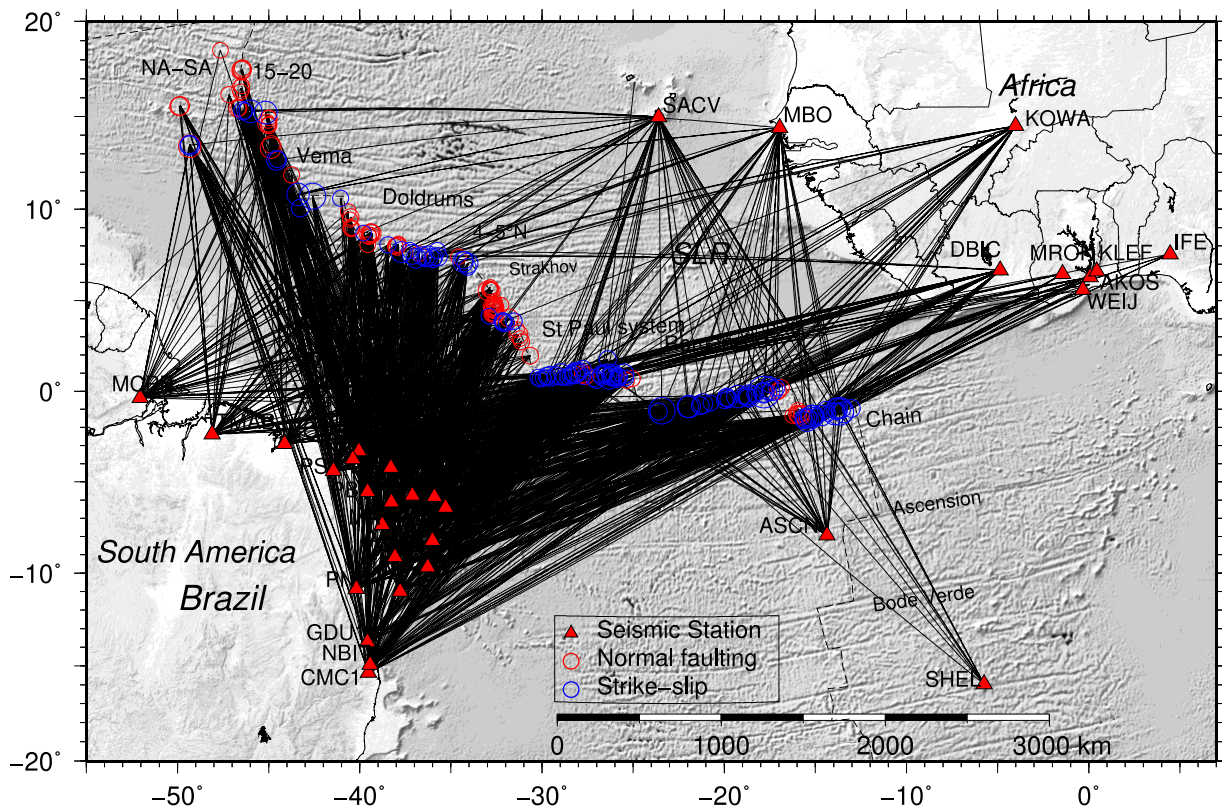**Figure 3.** *Pn* wave propagation paths between 189 earthquakes and 32 stations selected for analysis are plotted. Nearly all source–receiver paths are exclusively along the oceanic lithosphere with a small continental crustal leg at the stations, except for station KOWA, which has substantial continental lithospheric paths. 2 041 paths are plotted.

to given parameters and Δp is the matrix of parameter changes. The parameter changes ($\Delta \mathbf{p}$) are obtained by the generalized inverse technique (Wiggins 1972; Kim 1987).

4. RESULTS

4.1 *Pn* amplitude–distance curve and $m_b(Pn)$ scale for the equatorial Atlantic region

We used 2041 *Pn* peak amplitude measurements to determine the parameters C, E and the constants b (= 1.29) and K (= 2.44) in eq. (5). The resulting amplitude–distance curve, $1.29 \cdot \log 10$ $(100/\Delta) + 2.44$, for *Pn* waves from the least-squares inversion is plotted in Fig. 4. The $m_b(Pn)$ magnitude scale for the equatorial Atlantic region in the distance range 700–3700 km is then:

$$m_b(Pn) = \log_{10} A \,[\text{nm}] - 1.29 \log_{10}(100/\Delta)\,[\text{km}] + C + 2.44,$$
(6)

where the constant $K = 2.44$ replaces the initial value of $K = 2.04 + K_0$ in eq. (5). So, the constant that ties $m_b(Pn)$ to moment magnitude M_w is $K_0 = 0.40$. Eq. (6) can be used to assign magnitude for earthquakes with magnitude range M_w 3.5–7.0 that occur along the equatorial MAR in the 700–3700 km distance range in the equatorial Atlantic region.

In the case of only the western side of the equatorial MAR, the slope of the amplitude–distance curve is 1.68, and the constant $K = 1.88$, whereas the slope is 1.16 and the constant $K = 2.83$ in the eastern side of equatorial MAR (Table S2 and Figs S1, S2). This suggests that *Pn* amplitude in the oceanic lithosphere along the equatorial MAR to western Africa attenuates more rapidly than to northeastern Brazil, as will be seen later. The essence of the $m_b(Pn)$ scale is the amplitude–distance correction curve that is empirically derived for the *Pn* phase in the equatorial Atlantic region.

4.2 Station correction

Station corrections account for the site conditions at seismic stations used in magnitude calculation. The station corrections implicitly include an incorrect instrument gain constant used to measure the peak amplitude. The station magnitude corrections determined from the inversion are plotted in Fig. 5 with filled triangles and are listed in Table 1. The corrections range from 0.71 (IFE) to –0.55 (TMAB) magnitude units for the 32 stations. Four stations—IFE, TMAB, RCBR (0.53) and SBBR (–0.44), had the largest values. The stations along the equatorial MAR—ASCN (0.06), SHEL (0.30) and SACV (0.18) show moderate positive corrections. Stations in the northernmost coastal region of Brazil show negative correction
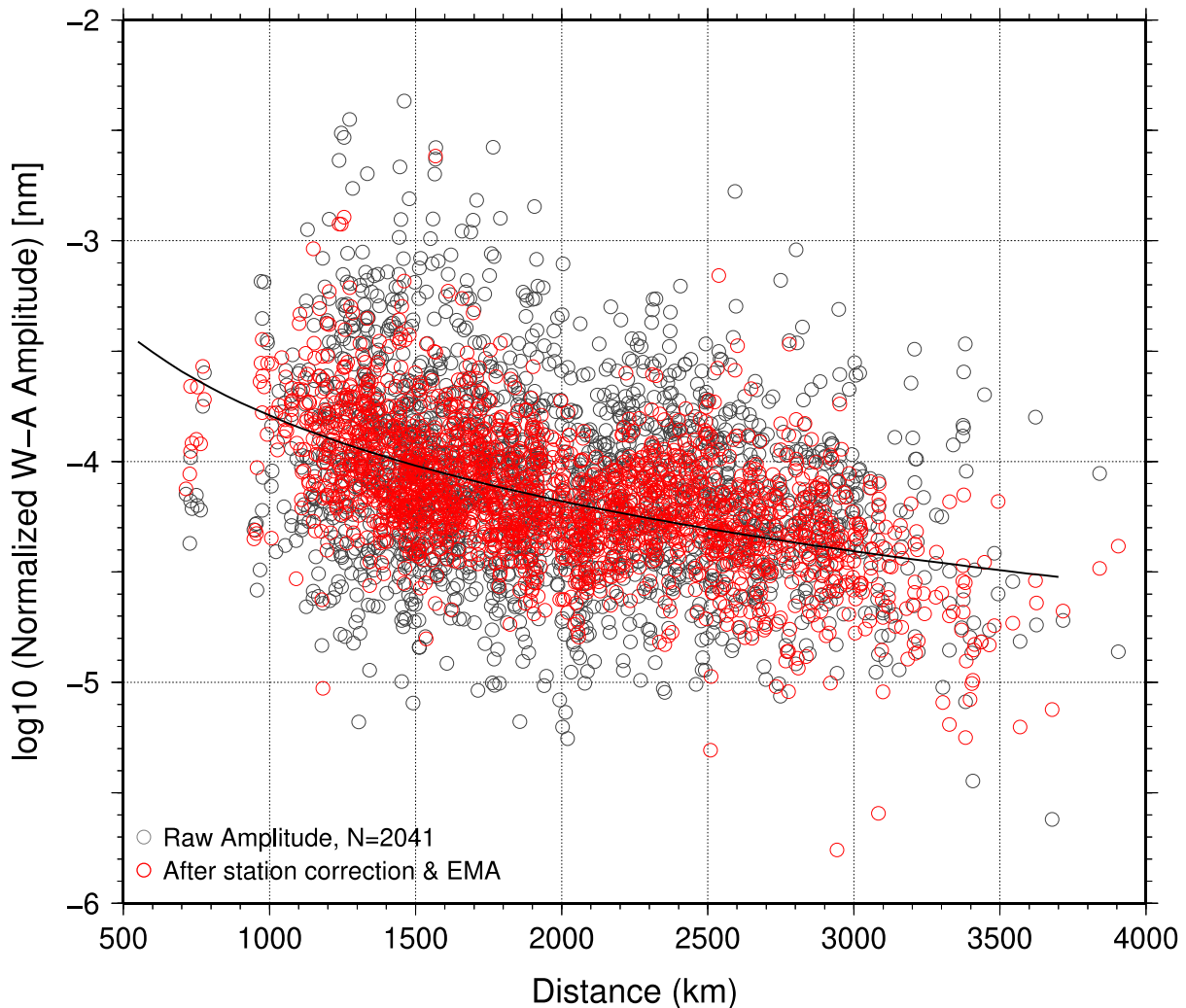
Pn, Wood–Anderson Peak Amplitudes

Figure 4. 2041 observed *Pn* peak amplitudes in nanometres are plotted against distance. The logarithm of peak amplitude normalized by subtracting the event moment magnitude M_w is plotted with *grey circles*. The calculated peak amplitudes in the least-squares inversion—after making station corrections and event magnitude adjustments (EMAs)—are plotted with *red circles* for comparison. The thick solid line is the amplitude–distance curve of *Pn* waves in the equatorial Atlantic region (eq. 6).

(*blue triangles*), and stations around easternmost Brazil show positive correction (*red triangles*) (Fig. 5). We found that the station corrections introduce a small scatter of about ±0.1 magnitude units in the $m_b(Pn)$ determination (see Fig. S8a). The network average $m_b(Pn)$ values calculated with and without the station corrections yield comparable M_w values (within 0.04 m.u.) over the magnitude range of M_w 4.95 to 7.14, as shown in Fig. S8. The station corrections have a negligible effect on network $m_b(Pn)$ determination, as shown in Fig. S8 (in the Supporting Information), probably due to the imposed condition that the sum of the corrections is zero.

Interestingly, the positive station corrections in easternmost Brazil (e.g. RCBR, NBPA, see Table 1) and the negative corrections along the northern coast of Brazil (e.g. MCPB, TMAB, ROSB and SBBR; see Fig. 5, Table 1), correlate quite well with upper

mantle *S*-wave anomalies of the SAAM23 model of Ciardelli *et al.* (2022): the strong and shallow asthenosphere in easternmost Brazil probably has higher attenuation and could explain the lower *Pn* amplitudes in that region (see Fig. S3). Similarly, high *S*-wave velocities in areas of thick lithosphere implies lower anelastic attenuation leading to negative station corrections. A similar correlation was found between station corrections with lithospheric thickness given by the CAM2016 model of Priestly *et al.* (2018), as shown in Fig. S3.

4.3 Event magnitude adjustments (EMAs)

The EMA is introduced to relate the *Pn* magnitude, $m_b(Pn)$ (short-period), to the moment magnitude, M_w (long-period). EMAs obtained range from –0.47 to 0.75 magnitude units with a standard
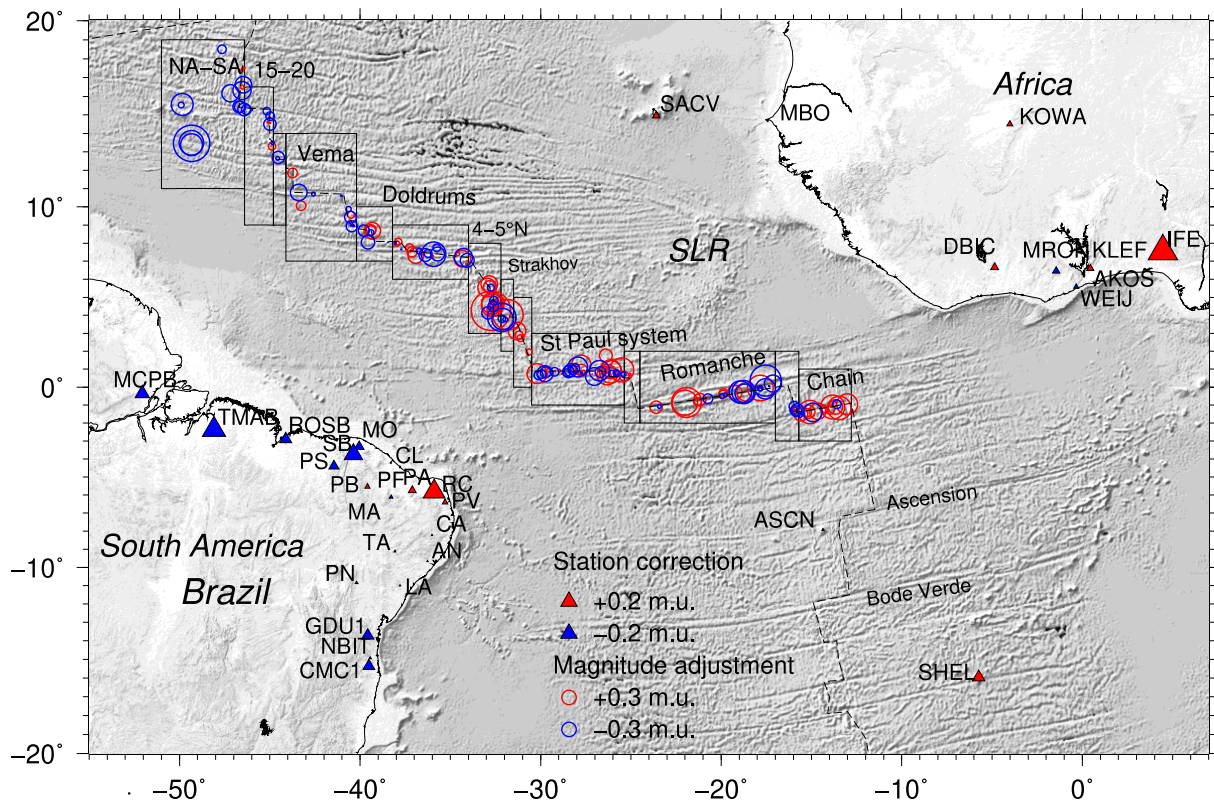
Figure 5. Event magnitude adjustments (EMAs) for 189 earthquakes and station corrections for 32 stations obtained from the inversion are plotted with symbols. Earthquakes on spreading ridges are mostly positive magnitude adjustments (red circles), whereas earthquakes on transform faults are mostly negative magnitude adjustments (blue circles). Stations in northeastern Brazil exhibit small positive station corrections (red triangles), and stations along the northern coastal region of Brazil reveal negative station corrections (blue triangles). Symbol size for the adjustments and corrections in magnitude units is scaled using the legend scale. Black rectangles represent 14 source specific regions along the equatorial MAR (see Table 2). Notice that station codes of Northeastern Brazil are denoted without the first two letters (NB), and two-letter station codes are used for—SB = SBBR, PF = PFBR and RC = RCBR.

deviation of 0.27 for 189 earthquakes (Table S1). The adjustment values are plotted in Fig. 5 with colour-coded circles. The earthquakes along transform faults situated north of the equator—Strakhov, Doldrums system south, Vema, Marathon and Fifteen-Twenty (15–20) as well as NA–SA (North America—South America) Plate boundary (see Fig. 1)—show negative event magnitude adjustments (*blue circles* in Fig. 5) consistent with northern MARs (Kim & Ottemöller 2017). However, earthquakes on the Chain transform fault south of the equator show positive values (*red circles* in Fig. 5), opposite to the cases in northern MARs reported by Kim & Ottemöller (2017).

Events on the narrow spreading ridges between the transform faults, Romanche—St Paul, St Peters—Strakhov, 4–5°N, and Doldrums—system north, are normal faulting events that show mostly positive values (*red circles*) consistent with the previous observation in the northern MARs (Kim & Ottemöller 2017). However, normal faulting events between Chain-Romanche (see Fig. 1) show negative EMA values.

These apparent discrepancies with previous results from the North Atlantic region could be explained by more complex structural features along the Chain- and Romanche-transform faults and normal faulting earthquakes between them close to the equator

(Fig. 5, e.g. Schilling *et al.* 1994; Gregory *et al.* 2023; Yu *et al.* 2023). Further, we recognize that earthquakes along the long transform faults close to the equator, Romanche and St Paul system, show a complex mix of positive and negative EMA values (Fig. 5), even though a majority of events have strike-slip faulting (Fig. 1). This could be explained by more complex geochemical and geodynamic features along the St Paul system, and Romanche transforms (Maia *et al.* 2016; Campos *et al.* 2022). In addition, a diversity of *Pn* velocities along these transform structures has been reported (e.g. de Melo *et al.* 2021b; see Text S1 in the Supporting Information).

4.4 Source specific magnitude adjustment (SSMA)

We obtained EMAs for each of the 189 earthquakes, but they do not apply to other earthquakes in the region or future earthquakes. However, we observed a trend of events along spreading ridges showing positive EMAs (red circles in Fig. 5) and earthquakes along the transform faults showing mainly negative EMAs (blue circles in Fig. 5) along the equatorial MAR. This systematic feature can be used to develop an approximation that can be applied to other events in the region (see Figs 1, 5 and Fig. S4).

Table 1. Station used and their station correction.

Station code	Network affiliation	Station correction (magnitude units)	Number of event data	Region
AKOS	GH	0.07	5	W Africa
ASCN	II	0.06	32	Ascension Island
CMC1	ON	− 0.27	75	NE Brazil
DBIC	GT	0.19	78	W Africa
GDU1	ON	− 0.29	80	NE Brazil
IFE	AF	0.71	5	W Africa
KLEF	GH	0.16	4	W Africa
KOWA	IU	0.14	40	W Africa
MBO	G	0.01	43	W Africa
MCPB	BR	− 0.34	54	N Brazil
MRON	GH	− 0.18	10	W Africa
NBAN	NB	0.03	89	NE Brazil
NBCA	NB	0.03	51	NE Brazil
NBCL	NB	0.02	115	N Brazil
NBIT	NB	0.06	54	NE Brazil
NBLA	NB	0.03	107	NE Brazil
NBMA	NB	0.00	125	NE Brazil
NBMO	NB	− 0.23	103	N Brazil
NBPA	NB	0.19	98	NE Brazil
NBPB	NB	0.12	128	NE Brazil
NBPN	NB	0.07	137	NE Brazil
NBPS	NB	− 0.25	124	N Brazil
NBPV	NB	0.13	72	NE Brazil
NBTA	NB	0.04	115	NE Brazil
PFBR	NB	− 0.09	8	NE Brazil
RCBR	IU	0.53	78	NE Brazil
ROSB	BR	− 0.29	49	N Brazil
SACV	II	0.18	65	Cabo Verde
SBBR	NB	− 0.44	16	N Brazil
SHEL	II	0.30	10	St Helena
TMAB	BR	− 0.55	63	N Brazil
WEIJ	GH	− 0.12	8	W Africa

BR = University of Brasilia Seismic Network; G = French Global Network of Seismological Broad-band Stations (GEO-SCOPE); GH = Ghana Digital Seismic Network; GT = Global Telemetered Seismograph Network (USAF/USGS); II = Global Seismograph Network—IRIS/IDA; IU = Global Seismograph Network—IRIS/USGS; NB = Northeastern Brazil UFRN and ON = Rede Sismográfica do Sul e do Sudeste.

Table 2. Source specific magnitude adjustment (SSMA) for the Equatorial Atlantic Region.

Source region	ST*	SSMA	S.D. †	No. of events	Lower left (°W, °N) Upper right (°W, °N)
Chain	T	0.174	0.248	18	(15.7°W, 3.0°S), (12.8°W, 1.0°N)
Chain–Romanche	S	− 0.161	0.110	5	(17.0°W, 3.0°S), (15.7°W, 2.0°N)
Romanche	T	0.002	0.349	24	(24.5°W, 2.0°S), (17.0°W, 2.0°N)
Romanche–St Paul	S	0.129	0.097	2	(25.38°W, 2.0°S), (24.5°W, 2.0°N)
St Paul system	T	0.004	0.266	37	(30.5°W, 1.0°S), (25.38°W, 3.0°N)
St Peters–Strakhov	S	0.181	0.105	5	(31.5°W, 0.0), (30.5°W, 5.0°N)
Strakhov	T	− 0.108	0.429	6	(32.2°W, 2.0°N), (31.5°W, 6.0°N)
4–5°N	S	0.131	0.242	25	(34.0°W, 3.0°N), (32.2°W, 8.0°N)
Doldrums system—south	T	− 0.033	0.223	22	(38.2°W, 6.0°N), (34.0°W, 9.0°N)
Doldrums system—north	S	0.019	0.241	7	(40.2°W, 7.0°N), (38.2°W, 10.0°N)
Vema	T	− 0.051	0.180	11	(44.1°W, 7.0°N), (40.2°W, 14.0°N)
Marathon	T	− 0.168	0.123	2	(44.8°W, 9.0°N), (44.1°W, 14.0°N)
Fifteen-Twenty (15°20')	T	− 0.072	0.126	10	(46.4°W, 9.0°N), (44.8°W, 16.5°N)
NA-SA Plate boundary	T	− 0.274	0.230	15	(51.0°W, 11.0°N), (46.4°W, 19.0°N)

*ST = Spreading ridges (S) or transform faults (T).
†S.D. = standard deviation.

We define 14 specific regions in the equatorial MAR based on (1) type of focal mechanism, (2) geological ridge segmentation and (3) bathymetric features. We assume that source type and, hence, magnitude adjustments are the same for all seismic events in each of these source specific regions. Each of the 14 regions has four sides defined by lines of constant latitude and longitude, as shown in Fig. 5 and Table 2. The transform faults from the south to north are (1) Chain, (2) Romanche, (3) St Paul system, (4) Strakhov, (5) Doldrums system–south, (6) Vema, (7) Marathon and (8) Fifteen-Twenty (15°20') transform faults and (9) NA-SA plate boundary, and five spreading
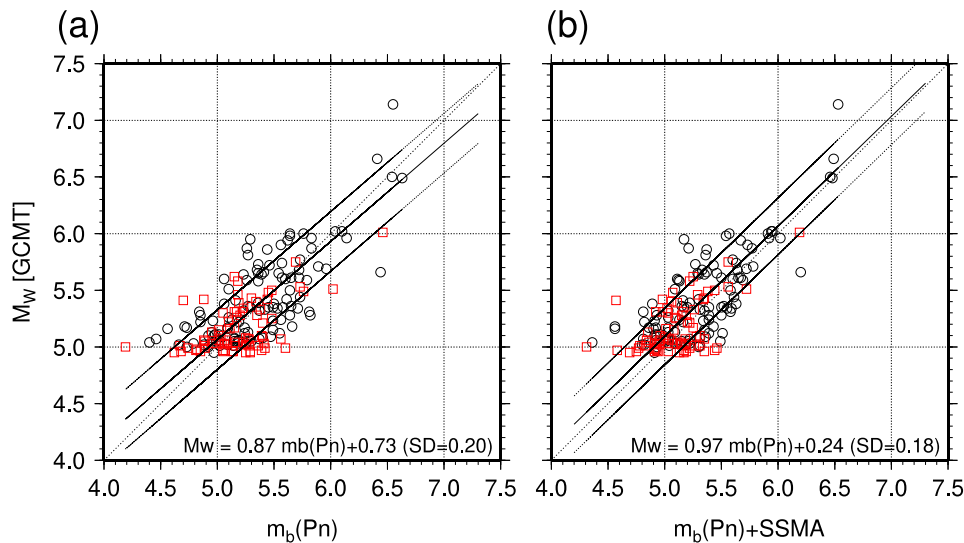
Figure 6. Comparisons of $m_b(Pn)$ and M_w values for 189 earthquakes. (a) $m_b(Pn)$ determined from the peak amplitude compensated only with the amplitude–distance curve. The regression line with a slope of 0.87 (centre solid line) and lines of one orthogonal standard deviation of 0.20 magnitude units (dashed lines) are drawn. (b) $m_b(Pn)$ determined after making our regional magnitude adjustment, SSMA, but no station corrections. The regression yields a slope of 0.97 with a standard deviation of only 0.18 magnitude units, indicating that a reasonably precise approximation to the moment magnitude in the range from M_w 3.5 to 7.0 is given by our values of $m_b(Pn)$ once the regional magnitude adjustment for various source regions is applied. Earthquake source types are indicated: normal (grey circles) and strike-slip (red squares).

ridges between these transform faults—(1) Chain–Romanche, (2) Romanche–St Paul, (3) St Peters–Strakhov, (4) Doldrums system–north and (5) 4–5°N.

We determined a source-region specific magnitude adjustment for each region by taking the mean of the EMAs of the events in each region (Fig. 5; Table 2). The 14 regional SSMA values range from −0.27 (NA-SA) to 0.18 (St Peters–Strakhov). The values are small but have large standard deviations (up to 0.43) (Table 2), reflecting a complex distribution of magnitude adjustments.

We find that SSMAs obtained for earthquakes along equatorial MAR for $m_b(Pn)$ show an overall average SSMA value of −0.09 ± 0.09 magnitude units that can be used for earthquakes along transform faults, whereas an average value of 0.12 ± 0.07 magnitude units can be assigned for events on spreading ridges. Events along the Chain transform fault may be assigned 0.17 ± 0.25 magnitude units and −0.16 ± 0.11 magnitude units for events along Chain–Romanche spreading ridge segments. The moment magnitude M_w can be determined from $m_b(Pn)$ by adding the appropriate SSMA values. We write an approximate M_w obtained from Pn for the jth event in the kth region on the equatorial MAR as

$$M_W(Pn)_{jk} = m_b(Pn)_j + \text{SSMA}_k. \tag{7}$$

5. DISCUSSION

5.1 Comparison of $m_b(Pn)$ and M_w

We calculated $m_b(Pn)$ for 189 earthquakes [without station corrections] using eq. (6) and compared them with moment magnitudes from the GCMT catalogue. A comparison between $m_b(Pn)$ and the moment magnitude, M_w is shown in Fig. 6(a). Regression between $m_b(Pn)$ and M_w yields $M_w = 0.87\,m_b(Pn) + 0.73$ with a

standard deviation of 0.20 magnitude units. The two magnitude values converge at magnitude 5.6. $m_b(Pn)$ correlates fairly well with M_w as indicated by the slope of 0.87, but there is some scatter in $m_b(Pn)$ and M_w values. Those events around M_w 5.0 have a greater scatter with $m_b(Pn)$ (see Fig. 6a). Many events with normal faulting mechanisms from the spreading ridges are in the narrow M_w range from 4.9 to 5.1 and show a wide range of $m_b(Pn)$ values. This is likely due to the earthquake source radiation effects manifested as the event magnitude adjustment discussed in the previous section.

The SSMAs provide improved $m_b(Pn)$ magnitudes to approximate the M_w values, as shown in Fig. 6(b). We find $m_b(Pn)$ + SSMA $\approx M_w$ over a wide range, M_w 4.9 to 7.1 within ±0.18 magnitude units without station corrections. In short, $m_b(Pn)$ represents ground motion amplitude due to high-frequency source radiation better than M_w, and the SSMA enables us to approximate the moment magnitude, M_w, by using $m_b(Pn)$ for earthquakes along the equatorial MAR.

5.2 Comparison of $m_b(Pn)$ amplitude distance curves

To develop the Pn magnitude scale for earthquakes that occur on equatorial MARs, we determined the amplitude–distance curve for Pn waves in the equatorial Atlantic region. The Pn amplitude distance curve for distances ranging from 700 to 3700 km is plotted in Fig. 7. In addition to the overall curve for all used data, we determined separate curves for the paths from the ridges to stations in Brazil (western paths) and to stations in Africa (eastern paths). The western paths show higher amplitudes, corresponding to less attenuation (*blue* dashed line in Fig. 7), whereas the curve for the eastern paths (towards Africa, Fig. 3) shows higher attenuation (*light brown* dashed line in Fig. 7). We note that the peak amplitude data for the eastern paths consist of only 378 observations, whereas 1663 peak amplitude data were available for the western paths as
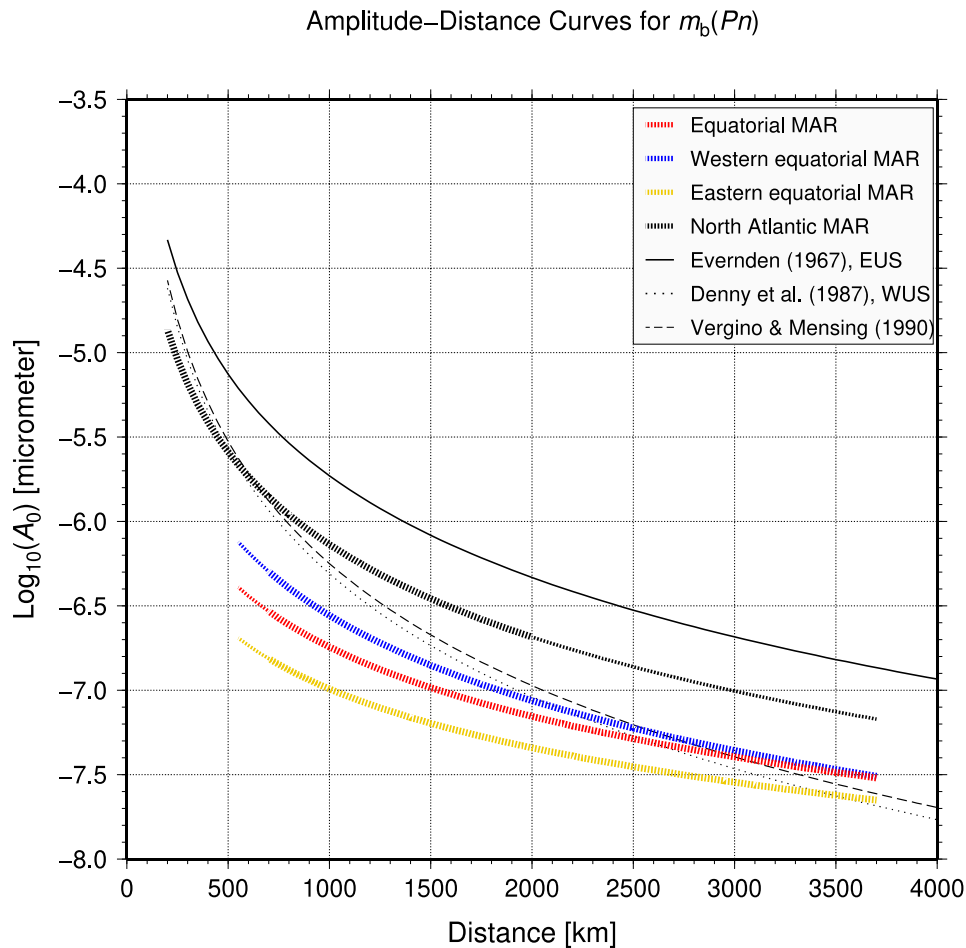
Amplitude–Distance Curves for $m_b(Pn)$

Figure 7. The amplitude–distance curves, $-\log_{10}(A_0)$, for $m_b(Pn)$ magnitude scale for the equatorial Atlantic region are drawn with thick dashed lines (700–3500 km). The curve for the paths from the ridges to stations in Brazil (western paths) shows less attenuation (blue dashed line), whereas the curve for the paths from the ridges to stations in Africa (eastern paths; Fig. 3) shows higher attenuation (light brown dashed line). The curve that includes both paths from the ridges to stations in Africa and Brazil shows comparable attenuation to the western paths (red dashed line). Amplitude–distance curves for various regional $m_b(Pn)$ scales normalized to the zero-to-peak amplitude in micrometres are plotted for comparison. The curves are for the North Atlantic region, eastern United States and western United States. The amplitude–distance curve for the Pn phase along the paths in the equatorial Atlantic region shows higher amplitude decay than that of the North Atlantic region (grey). Amplitude is about a factor of 4 smaller at 1000 km and becomes a factor of ~3 smaller at 2000 km than those of the Northern Atlantic region.

depicted in Fig. 3. Hence, the curve for the eastern paths may be less well-constrained. The curve for the western region of the equatorial Atlantic shows low attenuation of about 0.2 magnitude units at short distances, but the difference decreases with distance, and at 2000 km, it is only 0.1 magnitude units and is nearly identical at 3000 km (Fig. 7). We take the curve that includes all paths from both side of equatorial MAR as our standard amplitude distance curve for the equatorial Atlantic region.

Amplitude–distance curves for various regional $m_b(Pn)$ scales normalized to the zero-to-peak amplitude in micrometres are plotted in Fig. 7 for comparison. Pn curves plotted are for the northern Atlantic region (Kim & Ottemöller 2017), eastern United States. (Evernden 1967), and western United States (Denny *et al.* 1987; Vergino & Mensing 1990). The amplitude–distance curve for the Pn phase along the paths in the equatorial Atlantic region shows higher amplitude decay than that of the northern Atlantic region. Amplitude is about a factor of 4 smaller at 1000 km (~0.61 logarithmic units) and becomes a factor of ~3 smaller at

2000 km (0.48 magnitude units) than those of the Northern Atlantic region.

Our curve for Pn in the equatorial Atlantic region shows the highest amplitude decay with a distance up to about 2500 km and is comparable to those for Pn in the continental lithosphere of the western United States reported by Denny *et al.* (1987) and Vergino & Mensing (1990) (see Fig. 7). A high amplitude attenuation in the equatorial Atlantic region may be due to deep mantle hydration with water-induced mantle melting which has been observed in equatorial MAR (e.g. Wang *et al.* 2022). The hydration increases serpentinization and changes the seismic wave propagation characteristics in the uppermost mantle in the central area of the equatorial MAR (Gregory *et al.* 2021). On the other hand, the North Atlantic region studied by Kim & Ottemöller (2017) has low attenuation, as observed by the high Q-factor in the same area (Adenis *et al.* 2017).

The higher attenuation in the eastern paths, for instance, could be related to a mantle plume proposed beneath the Sierra Leone

Rise (SLR in Fig. 1; Schilling *et al.* 1994). A low *Q*-factor with higher attenuation was identified in SLR area approximately down to 150 km depth compared to the southern area in the South American tectonic Plate (Adenis *et al.* 2017). In addition, the difference in amplitude–distance curves between the eastern and the western equatorial Atlantic regions can be: (1) linked to the different lithospheric and asthenospheric settings existing in the two tectonic plates—South American and African plates, across the equatorial MAR in the equatorial Atlantic region (Fig. 7) and (2) due to average difference in *S*-wave velocity anomalies, because recent *S*-wave velocity models—SAAM23 (Ciardelli *et al.* 2022) and SAM2019 (Celli *et al.* 2020), show average lower velocities in the eastern side (Africa) at 150 km depth, as seen in Figs S5 and S6.

6. CONCLUSIONS

We have developed a robust regional short-period *Pn*-wave magnitude scale $m_b(Pn)$ for earthquakes along the equatorial MAR in the equatorial Atlantic region (eq. 6). It can be used to assign magnitude for small- to moderate-size earthquakes in the equatorial Atlantic in the distance range of 700–3700 km.

The EMA relates the short-period *Pn* magnitude $m_b(Pn)$ to the long-period moment magnitude M_w. In the northern Atlantic region, strike-slip earthquakes on transform faults have negative adjustments, whereas normal faulting earthquakes along spreading ridges showed positive ones. We find earthquakes along the equatorial MAR show a more complex pattern. The long transform faults—Romanche and St Paul system- show a mix of positive and negative values, which can be attributed to more complex geological features along transform faults in the equatorial Atlantic.

Estimated station magnitude corrections reflect the *S*-wave velocity anomaly in the upper mantle. Positive corrections for stations in easternmost Brazil correlate with the region's strong and shallow asthenosphere with high attenuation, whereas negative station corrections along the northern coast of Brazil relates to high *S*-wave velocities in a thick lithosphere with low anelastic attenuation.

Finally, the source-region specific magnitude adjustments—regionalized for 14 geographic regions, help in the use of $m_b(Pn)$ magnitudes to provide approximate M_w values. We find $m_b(Pn)$ + Regional magnitude adjustment $\approx M_w$ over a wide magnitude range of $m_b(Pn)$ 4.5–6.5 for earthquakes in the equatorial Atlantic region with a standard deviation of 0.18 magnitude units.

SUPPORTING INFORMATION

Supplementary data are available at *GJIRAS* online.

Text S1. Variations of *Pn* propagation in St Paul and Romanche transforms.
Table S1. List of earthquakes analysed.
Table S2. Inversion results.*
Figure S1. Attenuation curve for the Western part of the equatorial MAR, with 1663 observed *Pn* peak amplitudes in nanometres.
Figure S2. Attenuation curve for the Eastern part of the equatorial MAR, with 378 observed *Pn* peak amplitudes in nanometres.
Figure S3. Comparisons of station corrections and V_S distribution at a 150 km depth, and station corrections versus lithosphere–asthenosphere boundary (LAB) depths.
Figure S4. Correlation of the event magnitude adjustments (EMA) with the lithospheric thickness in the St Paul system and Romanche transform fault.

Figure S5. Comparison of the V_S distribution at 150 km depth and the amplitude–distance curves for western (towards Brazil) and eastern (towards African) paths.
Figure S6. Comparison of *S*-wave velocity distribution at 150 km depth from the tomography model SAM2019 (Celli *et al.* 2020) and *Pn* amplitude attenuation in the eastern and western sides of the equatorial MAR.
Figure S7. Comparisons of $m_b(Pn)$ and M_w values for 189 earthquakes with the event magnitude adjustment (EMA) and station corrections and without corrections.
Figure S8. Comparisons of $m_b(Pn)$ and M_w values for 189 earthquakes to examine the effect of station corrections.

Please note: Oxford University Press are not responsible for the content or functionality of any supporting materials supplied by the authors. Any queries (other than missing material) should be directed to the corresponding author for the article.

AUTHOR CONTRIBUTIONS

Won-Young Kim (Conceptualization [equal], Formal analysis [lead], Investigation [lead], Methodology [lead], Software [equal], Validation [equal], Visualization [equal], Writing – original draft [equal], Writing – review & editing [equal]); Guilherme W. S. de Melo (Conceptualization [supporting], Data curation [lead], Formal analysis [supporting], Funding acquisition [supporting], Investigation [supporting], Methodology [supporting], Project administration [lead], Validation [supporting], Writing – review & editing [supporting]) and Marcelo Assumpção (Conceptualization [supporting], Formal analysis [supporting], Investigation [supporting], Validation [supporting], Writing – review & editing [supporting]).

DATA AVAILABILITY

About half of the stations used in this study are in northeastern Brazil, operated by the Seismological Laboratory (LabSis) at the Federal University of Rio Grande do Norte, Natal, Brazil; UFRN). We used 15 stations operated by the network under network code NB (RSISNE) <https://labsis.ufrn.br/>. Three stations with network code BR operated by the Universidade de Brasília—UnB) <http://obsis.unb.br/portalsis/>; Two stations of the Observatorio Nacional with network code ON operating for south and southeast of Brazil (RSIS) <https://www.rsis.on.br/>. Data from the Seismology Center of the University of São Paulo (USP; BL, southeast) and other NB, BR, and ON networks of the Brazilian Seismographic Network can be obtained from request: https://www.rsbr.on.br/request. Data of five GSN stations (doi: 10.7914/SN/II) and (doi: 10.7914/SN/IU), and a station of the AfricaArray (AF at: https://ds.iris.edu/mda/AF/); four stations in Ghana (GH); a GeoScope station (G) and station DBIC operated by

USGS with network code GT were downloaded through the Earth-Scope Consortium Wilber 3 system (https://ds.iris.edu/wilber3/).

REFERENCES

Abercrombie, R.E. & Ekström, G., 2001. Earthquake slip on oceanic transform faults, *Nature,* **410,** 74–77.

Adenis, A., Debayle, E. & Ricard, Y., 2017. Attenuation tomography of the upper mantle, *Geophys. Res. Lett.,* **44,** 7715–7724.

Aki, K., 1966. Generation and propagation of G waves from the Niigata earthquake of June 16, 1964, *Bull. Earthq. Res. Inst., Univ. Tokyo,* **44,** 23–88.

Anderson, J.A. & Wood, H.O., 1925. Description and theory of the torsion seismometer, *Bull. seism. Soc. Am.,* **15,** 1–72.

Assumpção, M., 1983. A regional magnitude scale for Brazil, *Bull. seism. Soc. Am.,* **73,** 237–246.

Bianchi, M.B. *et al.*, 2018. The Brazilian seismographic Network (RSBR): improving seismic monitoring in Brazil, *Seismol. Res. Lett.,* **89,** 452–457.

Boatwright, J., 1994. Regional propagation characteristics and source parameters of earthquakes in northeastern North America, *Bull. Seism. Soc. Am.,* **84,** 1–15.

Bonatti, E., 1978. Vertical tectonism in oceanic fracture zones, *Earth planet. Sci. Lett.,* **37,** 369–379.

Bonatti, E., Ligi, M., Carrara, G., Gasperini, L., Turko, N., Perfiliev, S. & Sciuto, P.F., 1996. Diffuse impact of the Mid-Atlantic Ridge with the Romanche transform: an ultracold ridge-transform intersection, *J. geophys. Res.,* **101,** 8043–8054.

Campos, T.F., Bezerra, F.H., Srivastava, N.K., Vieira, M.M. & Vita-Finzi, C., 2010. Holocene tectonic uplift of the St Peter and St Paul Rocks (Equatorial Atlantic) consistent with emplacement by extrusion, *Mar. Geol.,* **271,** 177–186.

Campos, T.F., Sichel, S.E., Maia, M., Brunelli, D., Motoki, K., Magini, C. & de Melo, G., 2022. The singular St. Peter and St. Paul Archipelago, equatorial Atlantic, Brazil, in *Meso-Cenozoic Brazilian Offshore Magmatism,* pp. 121–165, Academic Press.

Celli, N., Lebedev, S., Schaeffer, A., Ravenna, M. & Gaina, C., 2020. The upper mantle beneath the South Atlantic Ocean, South America and Africa from waveform tomography with massive data sets, *Geophys. J. Int.,* **221,** 178–204.

Chun, K.Y., Kokoski, R.J. & West, G.F., 1989. High-frequency pn attenuation in the Canadian Shield, *Bull. seism. Soc. Am.,* **79,** 1039–1053.

Ciardelli, C., Assumpção, M., Bozdağ, E. & van der Lee, S., 2022. Adjoint waveform tomography of South America, *J. geophys. Res.,* **127,** e2021JB022575.

de Melo, G.W.S. & do Nascimento, A.F., 2018. Earthquake magnitude relationships for the Saint Peter and Saint Paul Archipelago, Equatorial Atlantic, *Pure appl. Geophys.,* **175,** 741–756.

de Melo, G.W.S., Mitchell, N.C., Zahradnik, J., Dias, F. & do Nascimento, A.F., 2021a. Oceanic seismotectonics from regional earthquake recordings: the 4–5°N mid-Atlantic ridge, *Tectonophysics,* **819,** doi:10.1016/j.tecto.2021.229063.

de Melo, G.W.S., Parnell-Turner, R., Dziak, R.P., Smith, D.K., Maia, M., do Nascimento, A.F. & Royer, J.-Y., 2021b. Uppermost mantle velocity beneath the Mid-Atlantic Ridge and transform faults in the Equatorial Atlantic Ocean, *Bull. seism. Soc. Am.,* **111,** 1067–1079.

DeMets, C., Gordon, R.G. & Argus, D.F., 2010. Geologically current plate motions, *Geophys. J. Int.,* **181,** 1–80.

Denny, M.D., Taylor, S.R. & Vergino, E.S., 1987. Investigation of mb and M_S formulas for the western United States and their impact on the Ms/mb discriminant, *Bull. seism. Soc. Am.,* **77,** 987–995.

Evernden, J.F., 1967. Magnitude determination at regional and near-regional distances in the United States, *Bull. seism. Soc. Am.,* **57,** 591–639.

Gregory, E.P., Singh, S.C., Marjanović, M. & Wang, Z., 2021. Serpentinized peridotite versus thick mafic crust at the Romanche oceanic transform fault, *Geology,* **49,** 1132–1136.

Gregory, E.P., Villinger, H., Singh, S.C. & Kaul, N., 2023. High heat flow anomaly within the St Paul Fracture Zone: heat advection and/or inherent thermal structure?, *Geochem. Geophys. Geosyst.,* **24,** e2022GC010385.

Kanamori, H., 1977. The energy release in great earthquakes, *J. geophys. Res.,* **82,** 2981–2987.

Kim, W.-Y. & Ottemöller, L., 2017. Regional *Pn* body-wave magnitude scale mb(Pn) for earthquakes along the northern mid-Atlantic Ridge, *J. geophys. Res.,* **122,** 10321–10340.

Kim, W.-Y., Ottemöller, L. & Richards, P.G., 2020. A regional Sn magnitude scale mb(Sn) and estimates of moment magnitude for earthquakes along the northern Mid-Atlantic Ridge, *Bull. seism. Soc. Am.,* **110,** 3158–3173.

Kim, W.Y., 1987. Modelling short-period crustal phases at regional distances for the seismic source parameter inversion, *Phys. Earth planet. Inter.,* **47,** 159–178.

Ligi, M., Bonatti, E., Gasperini, L. & Poliakov, A.N., 2002. Oceanic broad multifault transform plate boundaries, *Geology,* **30,** 11–14.

Maia, M. & Brunelli, D., 2020. The Eastern Romanche ridge-transform intersection (Equatorial Atlantic): slow spreading under extreme low mantle temperatures. Preliminary results of the SMARTIES cruise, in *Proceedings of the 22nd EGU General Assembly Conference,* held online 4-8 May 2020, id.10314.

Maia, M., Sichel, S., Briais, A., Brunelli, D., Ligi, M., Ferreira, N. & Oliveira, P., 2016. Extreme mantle uplift and exhumation along a transpressive transform fault, *Nat. Geosci.,* **9,** 619–623.

Priestley, K., McKenzie, D. & Ho, T., 2018. A lithosphere-asthenosphere boundary—a global model derived from multimode surface-wave tomography and petrology, in *Lithospheric Discontinuities,* pp. 111–123, eds Yuan, H. & Romanowicz, B., American Geophysical Union.

Richter, C.F., 1935. An instrumental earthquake magnitude scale, *Bull. seism. Soc. Am.,* **25,** 1–32.

Ringler, A.T. *et al.*, 2022. Achievements and prospects of global broadband seismographic networks after 30 years of continuous geophysical observations, *Rev. Geophys.,* **60,** e2021RG000749.

Schilling, J.G., Hanan, B.B., McCully, B., Kingsley, R.H. & Fontignie, D.,1994. Influence of the Sierra Leone mantle plume on the equatorial Mid-Atlantic Ridge: a Nd-Sr-Pb isotopic study, *J. geophys. Res.,* **99,** 12005–12028.

Sereno, T. & Orcutt, J.A., 1987. Synthetic pn and Sn wavetrains and the frequency dependence of Q of oceanic lithosphere, *J. geophys. Res.,* **92,** 3541–3566.

Uhrhammer, R.A. & Collins, E.R., 1990. Synthesis of Wood-Anderson seismograms from broadband digital records, *Bull. seism. Soc. Am.,* **80,** 702–716.

Vergino, E.S. & Mensing, R.W., 1990. Yield estimation using regional mb (Pn), *Bull. seism. Soc. Am.,* **80,** 656–674.

Vincent, C., Maia, M., Briais, A., Brunelli, D., Ligi, M. & Sichel, S., 2023. Evolution of a cold intra-transform ridge segment through oceanic core complex splitting and mantle exhumation, St. Paul Transform System, Equatorial Atlantic, *Geochem. Geophys. Geosyst.,* **24,** e2023GC010870.

Wang, Z., Singh, S.C., Prigent, C., Gregory, E.P. & Marjanović, M., 2022. Deep hydration and lithospheric thinning at oceanic transform plate boundaries, *Nat. Geosci.,* **15,** 741–746.

Wiggins, R.A., 1972. The general linear inverse problem: implication of surface waves and free oscillations for earth structure, *Rev. Geophys.,* **10,** 251–285.

Yu, Z., Singh, S.C. & Maia, M., 2023. Evidence for low vp/vs ratios along the eastern Romanche ridge-transform intersection in the equatorial Atlantic Ocean, *Earth planet. Sci. Lett.,* **621,** doi:10.1016/j.epsl.2023.118380.

Yu, Z., Singh, S.C., Gregory, E.P., Maia, M., Wang, Z. & Brunelli, D., 2021. Semibrittle seismic deformation in high-temperature mantle mylonite shear zone along the Romanche transform fault, *Sci. Adv.,* **7,** doi:10.1126/sciadv.abf3388.